Mineralized Collagen Fibrils: A Mechanical Model with a Staggered Arrangement of Mineral Particles

Ingomar Jäger* and Peter Fratzl*,†

*Institute for Metal Physics, University of Leoben, Erich Schmid Institute of Materials Science, Austrian Academy of Sciences, Leoben, and †Ludwig Boltzmann Institute of Osteology, Hanusch Hospital, Vienna, Austria

ABSTRACT   Both elastic modulus and fracture stress are known to increase with the amount of mineral deposited within collagen fibrils. Current mechanical models of mineralized fibrils, where mineral platelets are arranged in parallel arrays, reproduce the first effect but fail to predict an increase in fracture stress. Here, we propose a model with a staggered array of platelets that is in better agreement with results on molecular packing in collagen fibrils and that accounts for an increase of both elastic modulus and fracture stress with the amount of mineral in the fibril. Finally, we explore the dependence of the mechanical properties within the model, when the degree of mineralization and the thickness of the platelets as well as their distance varies.

INTRODUCTION

Bone is a hierarchically structured material with mechanical properties depending on its architecture at all levels of hierarchy (Carter and Hayes, 1977; Currey, 1984; Weiner and Wagner, 1998; Rho et al., 1998). The trabecular architecture, e.g., in the cancellous bone of vertebrae, strongly influences the stability of the structure. At a lower level of hierarchy, one has to consider the lamellar structure of the bone matrix, which renders the mechanical properties such as fracture toughness and elastic constants of bone extremely anisotropic. Finally, at the lowest level of hierarchy, bone matrix consists of mineralized collagen fibrils. Calcium phosphate (hydroxyapatite) nanocrystals are embedded into the collagen fibrils increasing their stiffness but decreasing their fracture strain. Because mineralized fibrils are the elementary unit of the complex bone structure, it is important to understand how their mechanical properties depend on the amount of mineral particles and their arrangement within the fibrils.

Mechanical models for bone have been studied for many years. In particular, the influence of bone mass distribution in cancellous bone, which mainly results from the trabecular architecture, can be predicted fairly accurately using finite element calculations (Huiskes and Hollister, 1993; Pettermann et al., 1997). In such calculations, however, bone matrix is usually approximated as an isotropic material, and anisotropic mechanical properties result from a preferred orientation of the trabeculae in cancellous bone (Kabel et al., 1999). Only recently, efforts were undertaken to include lower hierarchical levels and, in particular, the fibrillar nature of the bone matrix into mechanical models (Sasaki et al., 1991; Wagner and Weiner, 1992; Akiva et al., 1998). At

this level of description, it is not sufficient to consider a local mineral density but necessary explicitly to take into account the size, orientation, and local arrangement of the mineral particles in the collagen matrix.

It is obvious that the stiffness and fracture strain of bone tissue depend on the amount of mineral deposited in the collagen matrix. From a simple rule of mixture, one expects an increase in stiffness (but also brittleness) with increasing mineral density (Currey, 1969, 1984, 1990). At the level of individual fibrils, the mechanical properties will also depend on the precise arrangement of the crystals within the fibrils (Weiner and Wagner, 1998; Rho et al., 1998). Given the small diameter of these fibrils in the order of 200 nm (Parry and Craig, 1980), it is, at present, impossible to isolate individual mineralized fibrils to perform mechanical experiments. A fairly close approximation, however, is the mineralized turkey leg tendon (MTLT). In this structure, collagen fibrils are arranged in a parallel fashion, and they can be found with a varying degree of mineralization depending on the age of the animal. For instance, Landis et al. (1995) presented a systematical investigation of the mechanical properties of MTLTs at varying degrees of mineralization, and of bone. Thus, one common source of experimental scatter was eliminated by referring, as far as possible, to the same material. Their results are summarized in Table 1. One interesting feature of this measurement is the very low value of Landis et al.'s Young's modulus as compared to values from other sources (Abe et al., 1996). Nevertheless, it is clear that the apparent Young's modulus, E (for definition, see Fig. 1), increases enormously with the amount of mineral deposited in the collagen structure (up to a factor of 400!), however, at the cost of a decrease of fracture strain, ε_{max}, by a factor of up to 30. At the same time, the fracture stress, σ_{max}, increases slightly by a factor of up to 5. Even though some caution is necessary because MTLT is an assembly of many collagen fibrils that need not necessarily contain the same amount of mineral each, and because there is no conclusive proof that MTLT and bone show the same mineralization pattern (Fratzl et al., 1992,

TABLE 1 Values of mechanical data

Typical Values*			
Type of Tissue	Collagen	Min. Tendon	Bone
Degree of mineralization Φ	0	0.15	0.40–0.45
Young's modulus [MPa]	50	400–700	10000–20000
E', relative to collagen		8–15	200–400
Maximum elastic strain [%]	35	6–8	0.5–1.0
ε', relative to collagen		0.15–0.25	0.015–0.03
Maximum elastic stress [MPa]	20	30–40	100
σ', relative to collagen		1.5–2.0	5
Special Values†			
Type of Tissue		Deer Antler	Whale Bulla
Degree of mineralization Φ		0.38	0.72
Young's modulus [MPa]		7400	31300
E', relative to collagen		150	630

*Taken from Landis et al. (1995).
†Taken from Currey (1984).

FIGURE 1 Schematic of the stress–strain (σ versus ε) curve of collagen. The slope of the linear part is considered to represent the elastic modulus of the collagen molecules. The maximum strain ε_{max} and the maximum stress (load) σ_{max} are defined as the limits of the linearly elastic regime.

1996), it is important for any mechanical model of mineralized collagen fibrils to reproduce the effect of mineralization on all three quantities, E, ε_{max}, and σ_{max}.

In this paper, we further develop previous models for the mechanical properties of mineralized collagen fibrils (Wagner and Weiner, 1992) by introducing a staggered arrangement of mineral particles in agreement with the distribution of gaps in the collagen fibril (Veis and Sabsay, 1987; Landis et al., 1993; Hulmes et al., 1995). We derive approximate elastic constants and their dependence on the degree of mineralization and also estimate the maximum stress and strain of the composite. In particular, we show that, in terms of mechanical performance, a staggered arrangement of mineral particles is by far superior to a strictly parallel arrangement.

A COMPARISON OF DIFFERENT MODELS OF MINERAL ARRANGEMENTS

In a typical bone remodeling event, the collagen matrix is deposited first and then thin mineral particles are nucleated without a change in the overall volume, essentially by the replacement of water (Glimcher, 1987; Posner, 1987). This implies structural constraints for the arrangement of the mineral particles inside a collagen fibril, which have to be considered for the mechanical model of the mineralized fibril.

Structural considerations

Collagen fibrils are well known to be assemblies of parallel collagen molecules arranged with a longitudinal stagger according to the Hodge–Petruska scheme (Hodge and
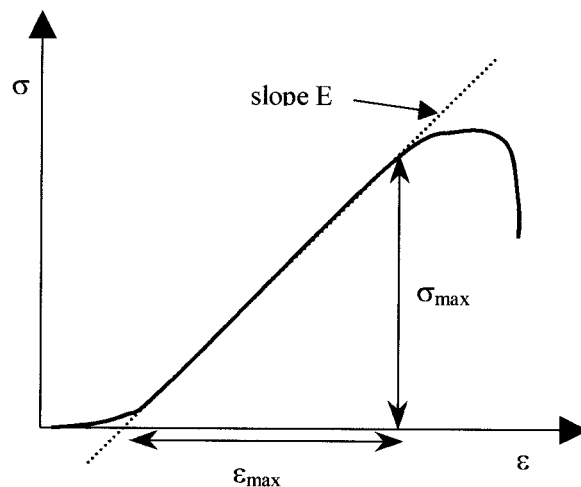
Petruska, 1963; Veis and Sabsay, 1987). A sketch of this structure is shown in Fig. 2 *a*. Because the length of the molecule (close to 300 nm) is not an integer multiple of the axial period (67 nm), the staggering leads to gaps in the structure. In fact, gap regions and overlap regions are arranged in a periodic fashion along the fibril, where the gap
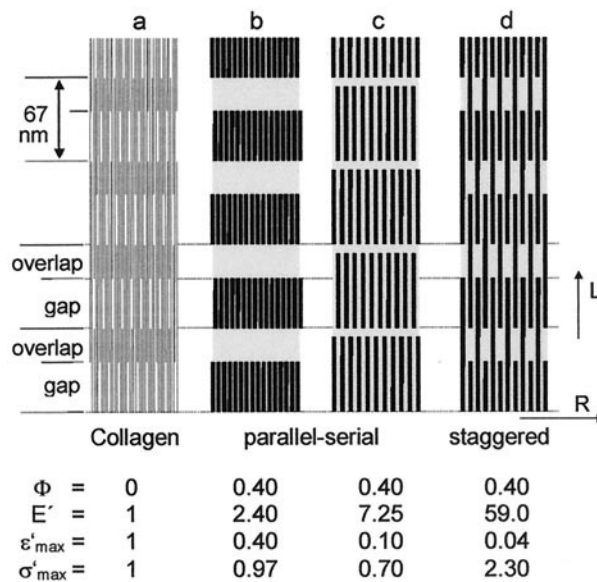

FIGURE 2 Comparison of two-dimensional models of mineral platelets in a collagen matrix. *a*, the Hodge–Petruska scheme of unmineralized collagen; *b–d*, different possibilities of the arrangement of mineral crystals. Arrows *R* and *L* denote the radial and longitudinal coordinate with respect to the arrangement shown in Fig. 3. The table shows the degree of mineralization, Φ, the elastic modulus, E', the maximum strain, ε'_{max}, and the maximum stress, σ'_{max}, for the arrangement above. All (primed) values are relative to the respective values of unmineralized collagen.

regions occupy roughly 60% and the overlap regions 40% of the axial periods. It is generally believed that mineral particles are nucleated primarily inside the gap region of the fibril where nucleation sites could be present and where more space is available since one-fifth of the collagen molecules are missing. In a later stage, however, the mineral particles extend into the overlap region. These particles are typically very flat (one dimension in the order of 2–4 nm (Fratzl et al., 1992, 1996; Weiner and Wagner, 1998) and elongated (the longest dimension may reach ≈ 100 nm) (Arsenault and Grynpas, 1988; Landis, 1995; Landis et al., 1996). This longest dimension is typically found to be oriented parallel to the collagen molecules in the fibrils.

Starting from the idea that the amount of mineral that can be deposited in the fibrils is limited by the amount of water in the unmineralized matrix that may be replaced by mineral, a number of constraints may be derived. Indeed, Lees (1987) has shown that the lateral spacing of the collagen molecules (i.e., the typical spacing in the direction denoted by R in Fig. 2) decreases both on drying and on mineralization, the smallest spacing being $d_{dry} = 1.1$ nm in fully dry collagen. The values for wet bone matrix are $d_{wet} = 1.55$ nm and for tibia $d_{bone} = 1.25$ nm. Changes in the axial period are also found but are much less dramatic (Fratzl et al., 1993) so that they need not be considered here. Hence, the largest possible volume fraction that may be incorporated into the overlap zone of the fibril corresponds to

$$\Phi_{overlap} < 1 - (d_{dry}/d_{wet})^2 \approx 0.50. \qquad (1)$$

A more likely estimate for bone is obtained using the actual spacing measured in compact bone,

$$\Phi_{overlap} \approx 1 - (d_{bone}/d_{wet})^2 \approx 0.35. \qquad (2)$$

Because one-fifth of the molecules are missing in the gap, a somewhat larger amount of mineral can be stored in the gap region,

$$\Phi_{gap} < 1 - 0.8(d_{dry}/d_{wet})^2 \approx 0.60, \qquad (3)$$

as the upper possible limit, and

$$\Phi_{gap} \approx 1 - 0.8(d_{bone}/d_{wet})^2 \approx 0.48, \qquad (4)$$

as the most likely value in fully mineralized bone. Considering that ~60% of each axial period is a gap region and the rest overlap, we get from these values an average mineral volume fraction in fibrils of $\Phi \approx 0.43$ in fully mineralized cortical bone and $\Phi = 0.56$ as the upper possible limit. These values are in good agreement with ash weight measurements of mineral content in bone (Abe et al., 1996). In any model for the mineralized collagen fibril, Eqs. 1–4 have to serve as boundary conditions.

Figure 2 shows several possible models for the deposition of mineral crystals in the fibrils. In Fig. 2 b, it is assumed that the crystals only occupy the gaps. This limits their length to about 40 nm. Typical values are assumed for the

thickness (3 nm) and for the overall mineral volume fraction ($\Phi = 0.40$). This implies that the mineral volume fraction in the gap is $0.40/0.6 \approx 0.67$, which is beyond the maximum possible value (Eq. 3). Hence, at this degree of mineralization the particles must extend into the overlap region.

In Fig. 2 c the crystals are assumed to grow into the overlap region to allow a reasonable mineral volume fraction of 0.45 in the gap region. The length of the crystals must then be about 60 nm and extend over most of the overlap region as well. The result is that the mineral density is practically the same in the gap and overlap region, which is clearly in contradiction to electron microscopy results (Glimcher, 1987; Landis et al., 1993; Weiner and Wagner, 1998) on single mineralized fibrils as well as to x-ray (Fratzl et al., 1993) and neutron scattering (White et al., 1977) data.

Fig. 2 d presents an arrangement where the crystals are even longer (~ 100 nm) but arranged in a staggered fashion. With the same overall mineral fraction $\Phi = 0.40$, we get the values $\Phi_{overlap} \approx 0.25$ and $\Phi_{gap} \approx 0.50$, which are not in contradiction to Eqs. 1–4. Moreover, the mineral content is higher in the gap than in the overlap region. Of course, Fig. 2 is only a 2-dimensional representation of the structure. A sketch for a possible 3-dimensional structure is given in Fig. 3. This is based on the proposal by Hulmes et al. (1995) that the gaps in the collagen fibril are arranged in concentric channels around the fibril core. For the rest of this paper, however, we stay within the two-dimensional description of Fig. 2.

Mechanical considerations

As shown schematically in Fig. 1, the stress versus strain curve of collagen is definitely nonlinear at the beginning ("toe" and "heel" region) due to the inherent kinks of the
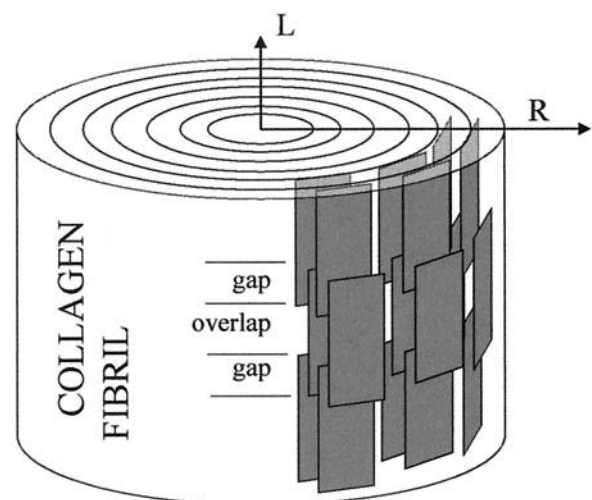

FIGURE 3   Sketch of the 3D arrangement corresponding to the staggered structure given in Fig. 2 d. The model is based on a concentric structure of the collagen fibril as proposed by Hulmes et al. (1995).

collagen fibrils and molecules (Vincent 1990; Misof et al., 1997; Fratzl et al., 1997). Therefore, the gradient of the central, more or less linear part of the curve, thought to represent the intrinsic properties of collagen molecules, is taken as the Young's modulus of pure, unmineralized collagen. Because, in the following, we restrict ourselves to purely elastic behavior, we define the maximum permitted strain and stress as the values at which the actual curve deviates significantly from the straight line drawn in Fig. 1. In other words, we associate the strain and stress at "failure" not with the actual breaking point of the material, but with the limit of elastic behavior (this is the model of an ideal elastic brittle material). With increasing mineralization, the toe and heel parts of the curve tend to diminish, and, for bone, cannot be found any more (Landis et al., 1995).

For the two parallel-serial models (Fig. 2, *b* and *c*), the elastic properties may be estimated using the Voigt–Reuss model discussed in the Appendix. Figure 2, *lower half*, gives E', σ'_{max}, and ε'_{max} for the models considered. All primed values of mechanical properties are normalized to the respective values of pure (unmineralized) collagen. Because the Young's modulus of hydroxyapatite is larger than that of collagen by three orders of magnitude, the mineral platelets are assumed to be infinitely stiff (rigid platelet model). The outstanding property of models *b* and *c* is that they are well able to yield an increase in E', but at the cost of a proportional decrease of ε'_{max}. Moreover, σ'_{max} can never extend beyond the value of pure collagen (which corresponds to $\sigma'_{max} = 1$) because the overall possible load is limited by the layers of unmineralized collagen appearing periodically along the fibril axis (Fig. 2, *b* and *c*). Therefore, the parallel-serial model cannot fully describe the properties of mineralized collagen. The staggered arrangement, in contrast, Fig. 2 *d*, does not suffer from that restriction. Because, in this case, a new source of strength is introduced, namely, shear stresses in the collagen phase between the overlapping mineral platelets, E' can be increased without losing a proportional amount of ε'_{max}. Consequently, the maximum load, σ'_{max}, is increased well beyond the value of unmineralized collagen, as will be shown in the next section.

FIBRIL WITH STAGGERED MINERAL CRYSTALS

In this model, estimates of mechanical properties using extensions of the rule of mixture must fail because the behavior is now dominated by shear in the matrix. A more refined but still simple treatment is therefore presented here, which leads ultimately to a closed-form solution. For the sake of simplicity, we will, in the following, replace the rather nonlinear and anisotropic collagen by an "effective" elastic medium with a Poisson's ratio of $\nu = 0.25$, as done by other authors, e.g., Akiva et al. (1998).

Figure 4 shows an enlarged view of an elementary cell of the staggered arrangement. In the longitudinal direction, the
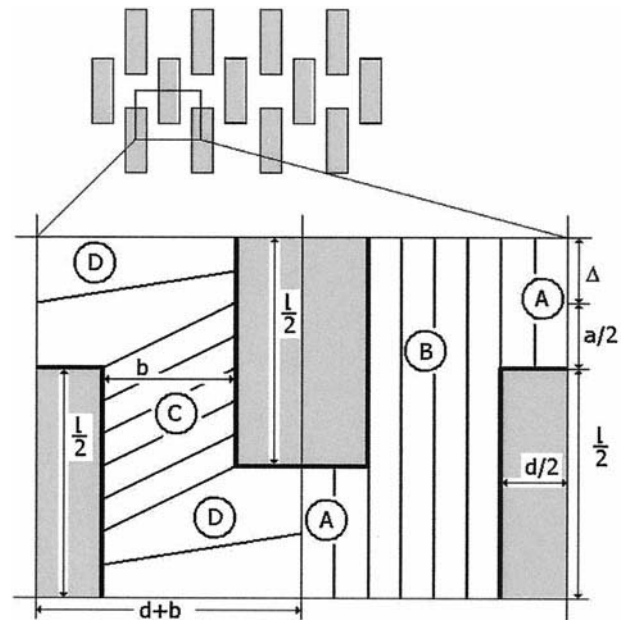

FIGURE 4 Two adjacent elementary cells of the staggered model showing the regions of tensile (regions *A* and *B*), and shear (regions *C* and *D*) stresses separately. The dimensions of the mineral, *l* and *d*, are indicated as well as the distances between them, *a* and *b*. The elementary cells are shown strained by an amount Δ.

cell of original length $(l + a)/2$ is elongated by an amount Δ, and the resulting force F is calculated on the basic (symmetry) plane with area $A = h(d + b)$ by superimposing tensile and shear stresses in the volumes indicated. All the dimensions (a, l, etc.) are defined in Fig. 4. Ideal coherence between mineral platelets and collagen at their respective interfaces is assumed. The tensile stress in region (A) and the shear stress in (C) are counted fully, whereas, of the tensile stress in (B) and the shear stress in (D), only appropriate fractions are counted. Using the principle that the average number of collagen molecules within a given cross-section of the fibril is not changed by mineralization (mineral replaces water within the fibril), the number of collagen molecules within an area $(b + d)h$ in unmineralized collagen will be approximately the same as within the area $b \cdot h$ between the crystals in Fig. 4. Hence, the effective elastic modulus of collagen in regions (A) and (B) of Fig. 4 is $\hat{E} \approx E_c (b + d)/b$, whereas the appropriate shear modulus used in regions (C) and (D), $\hat{G} = \gamma \hat{E}$ with $\gamma = 0.4$. To derive the relative elastic modulus, E', i.e., the elastic modulus of the composite relative to the elastic modulus of unmineralized collagen, the sum of the forces generated in regions (A)–(D), respectively, $F = F_1 + F_2 + F_3 + F_4$, is normalized by the force F_c exerted on the same area A by an equal amount of unmineralized collagen, given by

$$F_c = E_c \cdot (b + d) \cdot h \cdot \Delta/[(l + a)/2]. \qquad (5)$$

Thus, it is possible to compute the elastic modulus of the

composite relative to the modulus of unmineralized collagen by

$$E' = E/E_c = F/F_c = E_1 + E_2 + E_3 + E_4, \qquad (6)$$

where E_1 to E_4 are the contributions from regions (A) to (D), respectively:

A: Because the mineral platelets are assumed to be inextensible, the volume with cross-section dh is strained from length $a/2$ to $a/2 + \Delta$, yielding

$$E_1 = \hat{E} dh[\Delta/(a/2)]/F_c = d(l + a)/(ab). \qquad (7)$$

B: In this region, the tensile strain is distributed inhomogeneously because regions immediately adjacent to mineral crystals do not experience any tensile strain, assuming a tight binding between mineral crystals and the adjacent collagen molecules. Therefore, at the A–B boundary, the strain is concentrated in the short portion of length $a/2$ not adjacent to the mineral, whereas, in the center, the elongation can be distributed over the full length $(l + a)/2$. Assuming a roughly linear increase of strain between these extremes, the contribution from this region is

$$E_2 = \hat{E} bh\tfrac{1}{2}[2\Delta/a + 2\Delta/(a + l)]/F_c = (2 + l/a)/2. \qquad (8)$$

C: A slightly different subdivision is chosen to compute the shear strain. Here a volume with cross-section $h(l - a)/2$ is sheared by Δ/b, and, as long as $(l - a) \geq 0$, i.e., as long as there is any overlap of the mineral platelets, this results in

$$E_3 = \hat{G} h[(l - a)/2][\Delta/b]/F_c = \gamma(l - a)(l + a)/(4b^2). \qquad (9)$$

D: In this region, we assume that the sheared volume extends from the surface of one platelet toward the center line of the next mineral, a distance of $(b + d/2)$, instead of only b as in volume C. There are two such volumes considered, starting at the basic symmetry planes, bottom and top, where the shear strain is zero, whereas, adjacent to the mineral, it is $\Delta/(b + d/2)$. Taking the mean value over the cross-section, $ha/2$, leads to

$$E_4 = 2\hat{G} h(a/2)\tfrac{1}{2}[\Delta/(b + d/2)]/F_c$$
$$= \gamma a(l + a)/[2b(2b + d)]. \qquad (10)$$

The maximum permitted overall strain, ε'_{max} (normalized with its value for unmineralized collagen, ε^c_{max}), is given by the condition of not exceeding the maximum strain of collagen in any point (cf. Fig. 1). The individual strains within the volumes A–D are given in the text leading to Eqs. 6–10. In particular, the largest tensile strain occurs in region A, $\varepsilon_{tensile} = 2\Delta/a$. The largest shear strain occurs in region C, $\varepsilon_{shear} = \Delta/b$. Hence, the maximum strain is obtained by setting $\text{Max}\{\varepsilon_{tensile}, \varepsilon_{shear}\} = \varepsilon^c_{max}$, where, in the absence of experimental data, the maximum reversible shear strain of

collagen was assumed to be equal to the maximum reversible tensile strain, ε^c_{max}. Because the total tensile strain of the composite is just $2\Delta/(l + a)$, the normalized maximum strain becomes

$$\varepsilon'_{max} = [2\Delta/(l + a)]/\varepsilon^c_{max} = 2\,\text{Min}\{b, a/2\}/(l + a). \qquad (11)$$

Finally, the (normalized) maximum stress σ'_{max}, is determined as the product of the relative elastic modulus, E', and the maximum normalized strain, ε'_{max}.

CHOICE OF PARAMETERS AND LIMITS OF THE MODEL

Obviously, the model proposed has a number of degrees of freedom in the choice of the parameters: the dimension of the platelets, length l and thickness d, and a and b, the distances between them, even when Φ is fixed. In the two-dimensional model, Φ is connected to the linear dimensions as

$$\Phi(l + a)(b + d) = ld. \qquad (12)$$

The axial periodicity of the collagen structure with a period of 67 nm (cf. Fig. 2) imposes the additional condition,

$$(l + a)/2 = 67 \text{ nm}. \qquad (13)$$

These two relations effectively leave two free parameters in the problem, which we take to be d and b.

There are, however, some conditions that limit the possible variation of b and d. The limit $a = 0$ corresponds to mineral platelets extending continuously along the full length of the fibril. In such a case, ε'_{max} is given by the extensibility of the mineral alone, which has been set to 0 (rigid platelets) in the present approximate model. Moreover, the elastic modulus would become infinite with a approaching the value 0. Then, from Eq. 12, follows

$$a > 0 \Rightarrow d/(b + d) > \Phi. \qquad (14)$$

Second, when a becomes larger than l, there is no more staggering of the mineral particles (cf. Fig. 4) and layers of unmineralized collagen appear in between layers of mineralized collagen, similar to the case depicted in Fig. 2 c. Hence, for $a \geq l$, the arrangement no longer corresponds to the model of staggered mineral particles, and the method used to estimate the mechanical parameters, Eqs. 6–11, fails. We therefore consider only the case $a \leq l$, which gives (using Eq. 12)

$$a \leq l \Rightarrow d/(b + d) \leq 2\Phi. \qquad (15)$$

Furthermore, some algebra shows that, in the staggered model, one has the general expression,

$$\Phi \leq \Phi_{gap} \leq \tfrac{5}{4}\Phi \qquad (16)$$

When $a = 0$ or $a = l$, then the inequality becomes the equality $\Phi_{gap} = \Phi$. The other limit, $\Phi_{gap} = \frac{5}{4}\Phi$, is obtained exactly for the situation depicted in Fig. 2 d, where the mineral density in the gap is just twice that in the overlap. Hence, as long as the overall mineral density Φ is smaller than 0.48, Eq. 3 is automatically fulfilled. Because $\Phi = 0.6\Phi_{gap} + 0.4\Phi_{overlap}$, Eq. 15 also implies that

$$\frac{5}{8}\Phi \leq \Phi_{overlap} \leq \Phi, \tag{17}$$

and Eq. 1 is also automatically satisfied for $\Phi < 0.48$. Therefore, in the following, we only consider the case where $\Phi \leq 0.48$.

RESULTS

Typical results for a high degree of mineralization ($\Phi = 0.42$, roughly corresponding to fully mineralized bone) and low mineralization ($\Phi = 0.15$, mineralized tendon) are shown in Figs. 5 and 6, respectively, assuming a typical thickness for the mineral platelets, $d = 3.5$ nm, observed in a number of tissues (see, e.g., Fratzl et al., 1996). The upper graph shows the relative stiffness of the tissue E', and the
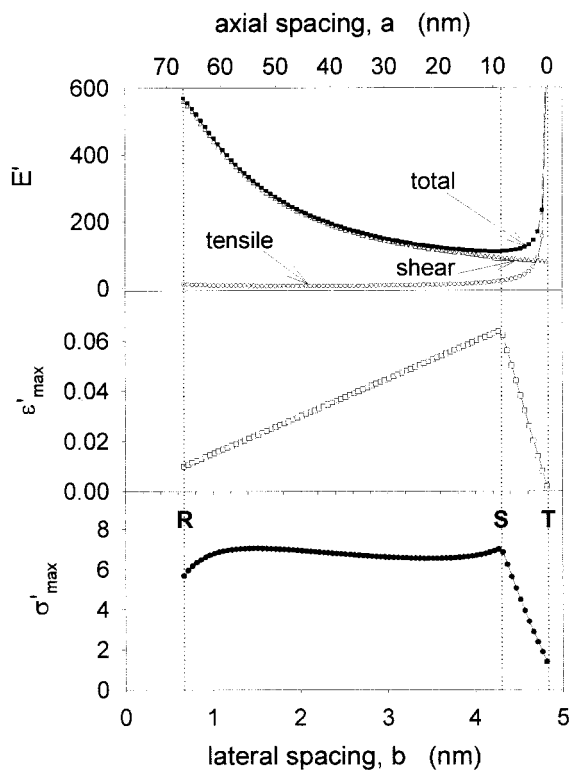
FIGURE 6 Same as Fig. 5, but calculated for $\Phi = 0.15$ and $d = 3.5$ nm, versus b.

FIGURE 5 Results for the elastic modulus, E', the tensile and shear part thereof, the maximum strain, ε'_{max}, and the maximum stress, σ'_{max}. All primed values relative to the respective values of unmineralized collagen, calculated for a mineralization $\Phi = 0.42$ and $d = 3.5$ nm, versus b. The limits denoted R, S, and T correspond to the cases $a = l$, $a = 2b$, and $a = 0$, respectively.
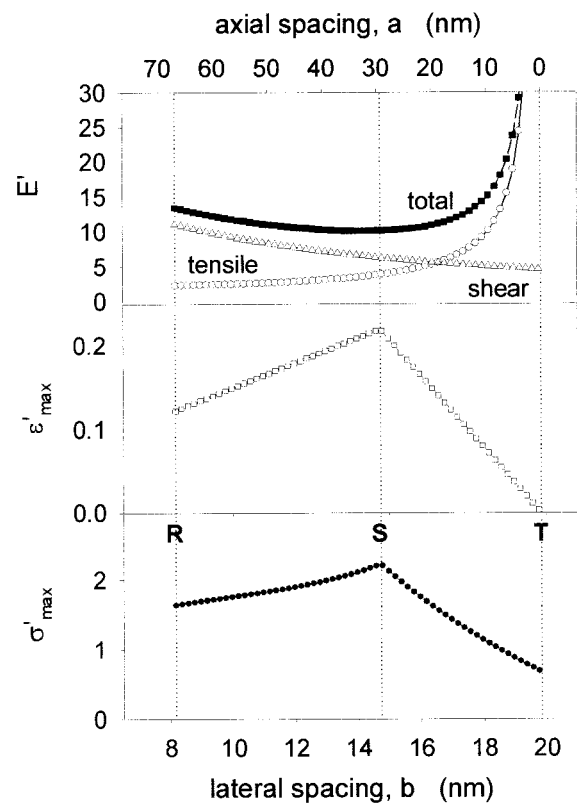
contributions due to shear, $E_3 + E_4$ (Eqs. 9 and 10) and to tensile strain, $E_1 + E_2$ (Eqs. 7 and 8). The central graph gives the maximum strain, ε'_{max}, and the lowest one the maximum stress, σ'_{max} (all quantities being normalized with respect to unmineralized collagen). These values are plotted as functions of the spacing between mineral platelets, b. From Eqs. 12 and 13, it can be seen that, for fixed Φ and d, varying b implies varying both a and l. Corresponding values of a are shown in Figs. 5 and 6 *top*, and the platelet length, l, is given by a through Eq. 13. It is clearly apparent in both Figs. 5 and 6 that the behavior at small average spacing between crystals is dominated by shear of the collagen matrix, whereas, for a larger spacing, it is dominated by tensile strains. The boundary between these types of behavior is the line labeled S, where shear and tensile strains in the collagen matrix are just equal, that is, $a = 2b$ according to Eq. 11. The limits T and R correspond to the inequalities $0 < a$ and $a \leq l$ (Eqs. 14 and 15, respectively). Accordingly, ε'_{max} and σ'_{max} correspond to shear failure between R and S and to tensile failure between S and T.

The steep decrease of ε'_{max} and σ'_{max} from S to T and the sharp increase of E' in the same region are connected to the fact that, here, the longitudinal distance between platelets, a, decreases sharply. At the limit of $a = 0$ (line T), one would have continuous mineral ribbons across the full length of the

fibril and the behavior would be dominated by the properties of the mineral (that is, extremely large stiffness, vanishing extensibility).

For a smaller lateral spacing between mineral platelets (region between R and S) the behavior is completely dominated by shearing of the collagen matrix. This is true not only for ε'_{max} and σ'_{max}, but also for the stiffness, where the shear contribution is by far dominating (particularly at higher mineral densities, Fig. 5). In this region, σ'_{max} is only weakly dependent on the spacing, b, and also the stiffness varies more gradually. Typically, the stiffness is largest for the smallest possible b. In the case of high mineral density (Fig. 5), the lowest value of b (at the limit R) is somewhat unrealistically small. Indeed, considering the number of collagen molecules that have to be present between the platelets (see Fig. 2 a), and squeezing them to the smallest possible volume (corresponding to a lateral spacing between molecules as in fully dry collagen) a spacing no smaller than $b_{min} = 1.6$ nm can be obtained. Hence, we expect that the largest relative stiffness to be obtained with $\Phi = 0.42$ (Fig. 5) would be ~300 (for $b = b_{min}$) together with a relative tensile stress of about 6. Similar values for the stiffness could also be obtained with a configuration where tensile strains in the matrix dominate (larger lateral spacing, b, but very small axial spacing, a), however, at the cost of a much smaller tensile stress!

At the lower mineral density $\Phi = 0.15$ (Fig. 6), the dependence on the spacing between crystals is generally weaker, and one can expect E' between 10 and 15 and σ'_{max} around 2. Only when the axial spacing decreases to zero (T), the stiffness increases but at the cost of a decrease in σ'_{max}.

To get a more complete picture, we have also plotted the same data as in Figs. 5 and 6 for different values of the crystal thickness, d. The convention is here to plot contour lines with the same value of E', ε'_{max}, and σ'_{max} (Fig. 7 and 8). For a fixed volume fraction of mineral, Φ, only two parameters remain in the model, given the relations in Eqs. 12 and 13. Hence, each of Figs. 7 and 8 explores the full parameter space of the model for $\Phi = 0.42$ and $\Phi = 0.15$, respectively.

At $\Phi = 0.42$ (Fig. 7, *top*) one can see that the maximum of E' always appears at the smallest d, but the dependence on b is ambivalent: starting from the minimum approximately at the S line, one can increase the elastic modulus either by enlarging or by decreasing b. Decreasing b means larger shear stress in the collagen matrix. Increasing b, in contrast, corresponds to a decrease of the spacing a, as discussed above, and always leads to extremely small maximum tensile stresses (between lines S and T in the lower part of Fig. 7).

E' and ε'_{max} for $\Phi = 0.15$ (Fig. 8), at first glance, look rather similar to the case above, the lower absolute values of E' compared to Fig. 7 are, of course, due to the lesser degree of mineralization, likewise the larger absolute values of ε'_{max}. But now the tensile and shear stress components along
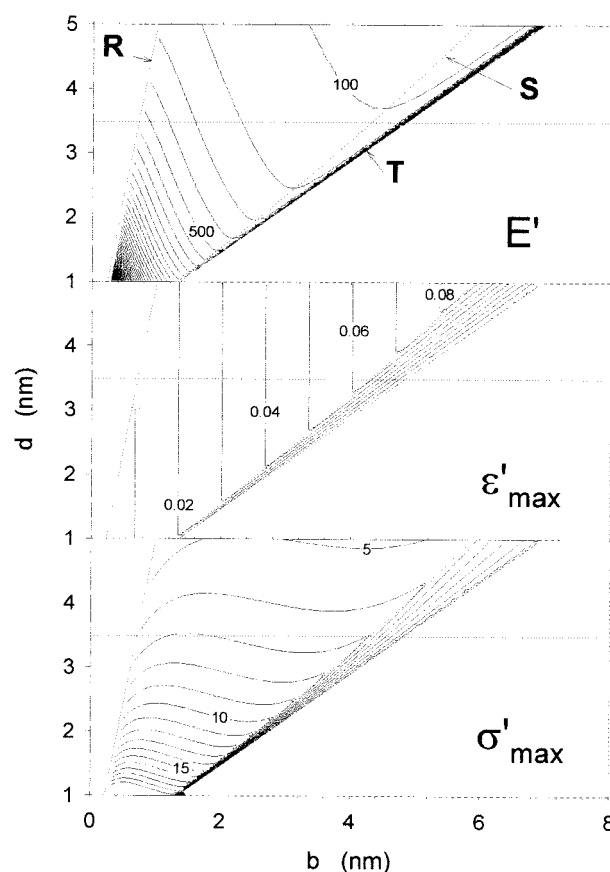

FIGURE 7 Contour plots of the elastic modulus, E', the maximum strain, ε'_{max}, and the maximum stress, σ'_{max} for a mineralization $\Phi = 0.42$. The limits denoted R, S, and T correspond to the cases $a = l$, $a = 2b$, and $a = 0$, respectively. The value $d = 3.5$ nm used in Fig. 5 is indicated by the horizontal dotted line.

the S line are more similar, so an equipartition of strain combined with a near-equipartition of stress between shear and tension leads to a different behavior of σ'_{max}: the maximum tensile stress, σ'_{max}, has a pronounced maximum along S, where the permitted strain, ε'_{max}, is largest, increasing with decreasing d, but at medium values of b.

In conclusion, we observe that the stiffness can increase by reducing either the lateral spacing, b, or the axial distance, a, between crystals. However, only the first of the two possibilities also leads to an increase in fracture stress as found in experiments on tendon and bone.

DISCUSSION

In mechanical models for mineralized collagen fibrils, it is not sufficient to consider only the stiffness of the tissue. Indeed, fracture strain and fracture stress are important characteristics and are likely to decrease when the stiffness is increased by mineralization. Here we have studied a model with a staggered arrangement of mineral particles distributed unequally in the gap and the overlap zone of the
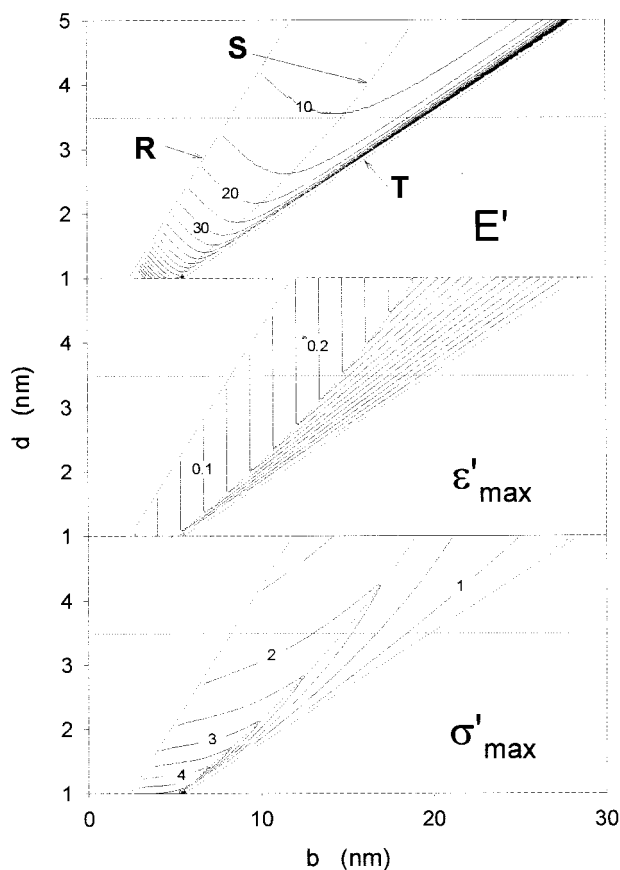
FIGURE 8   Same as Fig. 7, but for $\Phi = 0.15$. The value $d = 3.5$ nm used in Fig. 6 is indicated by the horizontal dotted line.

fibrils. This structure is not only consistent with recent models for the packing of collagen molecules within fibrils (Hulmes et al., 1995), but has also quite interesting mechanical properties. Due to the staggering, the collagen matrix feels tensile as well as shear stresses.

With a fixed volume fraction of mineral, Φ, the model is described by two parameters only, for example, the lateral spacing between mineral platelets, b, and their axial spacing, a. The most remarkable result is that the stiffness of the tissue (for given mineral content) increases when either spacing, b or a, decreases. The implications of these two cases are, however, extremely different, particularly at large Φ (e.g., $\Phi = 0.42$, which roughly corresponds to bone):

1. When the axial spacing, a, decreases, the behavior is dominated by tensile stress in the collagen layer between the column of crystals in axial direction of the fibril. It is clear that the stiffness increases when this layer decreases in thickness. The failure load of the mineralized fibril will, however, be dictated by the failure of the collagen layer in between the crystals. The model calculations (see Fig. 5) show clearly that a stiffness corresponding to the values found in bone (see Table 1) would

correspond to a failure load much smaller than found experimentally.

2. When, instead, the lateral spacing b decreases, the mechanical behavior starts to be dominated by shear of the collagen matrix in the layers between crystals staggered laterally. The model calculations show, in this case, that both the stiffness and the fracture load may increase significantly with mineralization and ultimately describe the typical experiment data for bone (Table 1).

In previous models (Wagner and Weiner, 1992; Akiva et al., 1998), parallel arrays of mineral platelets were assumed inside the fibrils. This leads to a succession of mineralized and unmineralized layers along the fibrils. To achieve a stiffness corresponding to the values found in bone, an extremely small axial spacing (about one Angstrom) had to be assumed between the mineral layers. Such a value is unrealistic given the typical thickness of collagen molecules. Moreover, the situation in such a Voigt–Reuss model corresponds roughly to case 1, in that the fracture load cannot exceed the one of unmineralized collagen. Clearly, the staggered model studied in the present paper is superior in describing the properties of bone tissue.

Interestingly, our model is also able to predict accurately the mechanical data for mineralized turkey leg tendon (Landis et al., 1995), when choosing the appropriate mineral density $\Phi = 0.15$ and a typical thickness of mineral crystals $d = 3.5$ nm. The model then predicts $E' = 10–15$, $\varepsilon'_{max} \approx 0.2$ and $\sigma'_{max} \approx 2$, for any reasonable value of b, in good agreement with the data in Table 1.

Table 1 also gives numerical values for deer antler (Currey, 1984). This tissue has a slightly lower degree of mineralization than bone ($\Phi = 0.38$), but a much smaller stiffness. Again, this can be reproduced easily within the framework of our model. This may be seen in Fig. 5 (drawn for $\Phi = 0.42$), which would not be much different for $\Phi = 0.38$. One can see that the stiffness is dramatically reduced but the fracture strain at the same time increased, when b is chosen at the S position rather than as small as possible. The values read in Fig. 5 for the stiffness at S are not far from those reported in the literature for deer antler (Table 1). Hence, one may speculate that the optimization of fracture strain rather than stiffness may lead to a tissue closer to antler than to bone (for a given volume fraction of mineral). This difference would be achieved by a somewhat larger lateral spacing of the crystals corresponding to the S point (Fig. 5), where the maximum tensile and shear strains appearing in the collagen matrix would just be equal.

Finally, data for bulla (Currey, 1984) are also included in Table 1. These rather small bones have a mineral volume fraction of $\Phi = 0.72$, which is well beyond the limits permitted in our model (Eqs. 1 and 3). Therefore, it must be assumed that part of the mineralization is found outside the fibrils where its contribution to the mechanical properties is

difficult to estimate. The high elastic modulus $E' \approx 630$ (see Table 1) can be reproduced using the present model even assuming an intra-fibrillar mineralization of only $\Phi = 0.48$ simply by choosing $b = b_{\min} = 1.6$ nm (in the absence of any measurements of mineral platelet dimensions for this rather special tissue, this assumption may be true) but then both b and d are at their respective minimum values, and, in addition, a is rather small, so that, for this case, the assumption of rigid platelets is no longer valid. Hence, for this case, other mechanisms for increasing the stiffness must be invoked.

One of the main results is also that the stiffest tissue is obtained for the thinnest possible crystals spaced laterally as tightly as possible. This corresponds well to the experimental observation that bone crystals are extremely thin with a width of only a few nanometers (Fratzl et al., 1992, 1996). What may seem surprising, however, is that this thickness is usually found to increase during bone maturation (Fratzl et al., 1991; Rinnerthaler et al., 1999). However, this does not mean a reduction of stiffness during maturation. On the contrary, if the number density of crystals is fixed for a given tissue, e.g., by the density of nucleation centers for the crystals (Glimcher, 1987), then $b + d$ is constant, and any increase in d leads to an increase in E', as visible, e.g., in Fig. 7.

Despite these encouraging results of the comparison between model calculations and experiment data, the significance of the numerical agreement should not be overestimated. First, data from mechanical experiments are reported for the entire tissue, which has a complex hierarchical structure and where the mineralized fibrils are only a motif used for building higher-order elements (e.g., lamellae) (Weiner and Wagner, 1998). Second, our calculations were done assuming the mineral platelets to have an infinite stiffness. In view of the elastic modulus of hydroxyapatite being at least three orders of magnitude larger than that of collagen, this seems to be quite natural. As long as neither spacing, a or b, approaches zero, the approximation remains valid. The limit when $a = 0$ or $b = 0$, however, leads to infinite stiffness, which is, of course, unreasonable. Third, our model is explored with very rough approximations of the actual mechanical behavior and is only two-dimensional.

Nevertheless, we believe that our numerical study has shown that a staggered arrangement of mineral particles in the fibrils is mechanically superior to a strictly parallel arrangement. Moreover, the model predicts the dependence of stiffness and fracture load on the volume fraction and spacing of mineral particles, which is in reasonable agreement with experimental data. A refinement of the model would require a three-dimensional treatment of the problem (as outlined in Fig. 3) and more accurate numerical computations using, e.g., finite element methods. Finally, of course, the influence of higher hierarchical bone structures (e.g., lamellae, osteons, etc.) needs to be considered.

APPENDIX: THE SERIAL-PARALLEL (VOIGT–REUSS) MODEL

It is well known that the properties of collagen–mineral composites like tendon and bone lie between the limiting cases of the Voigt (or parallel) and the Reuss (or serial) models (Currey, 1984). If we denote the volume fraction of mineral by Φ, then, for the parallel model, Young's modulus is composed from the moduli of the constituents collagen (index coll) and mineral (index min):

$$E_{\text{parallel}} = E_{\min}\Phi + E_{\text{coll}}(1 - \Phi), \quad (A1)$$

while the strains in mineral and collagen are identical and therefore limited by the more brittle component, i.e., the mineral,

$$\varepsilon_{\max,\text{parallel}} = \varepsilon_{\max,\min}. \quad (A2)$$

For the serial model, the compliances (the reciprocal values of the moduli) are additive,

$$1/E_{\text{serial}} = 1/E_{\min}\Phi + 1/E_{\text{coll}}(1 - \Phi), \quad (A3)$$

while the stresses are identical and therefore limited by the weaker phase, the collagen,

$$\sigma_{\max,\text{serial}} = \sigma_{\max,\text{coll}}. \quad (A4)$$

The maximum strain here is simply given by

$$\varepsilon_{\max,\text{serial}} = \sigma_{\max,\text{serial}}/E_{\text{serial}}. \quad (A5)$$

A series combination of layers of parallel platelets and layers of unmineralized collagen (index sp), as used, e.g., by Akiva et al. (1998), with a volume fraction of the reinforced phase β then yields

$$\frac{E_{\text{sp}}}{E_{\text{coll}}} = \frac{\Phi E_{\min} + (1 - \Phi)E_{\text{coll}}}{\beta E_{\text{coll}} + (1 - \beta)[\Phi E_{\min} + (1 - \Phi)E_{\text{coll}}]}. \quad (A6)$$

Because $E_{\text{coll}}/E_{\min} = \varepsilon \ll 1$,

$$\frac{E_{\text{sp}}}{E_{\text{coll}}} = \frac{\Phi + \varepsilon(1 - \Phi)}{\beta\varepsilon + (1 - \beta)[\Phi + \varepsilon(1 - \Phi)]} \quad (A7)$$

can be expanded yielding (as long as $\Phi \gg \varepsilon$)

$$\frac{E_{\text{sp}}}{E_{\text{coll}}} = \frac{1}{1 - \beta}. \quad (A8)$$

Therefore, it can be seen that, in this case, arbitrary increases in E_{sp} can easily be achieved by choosing a suitably small thickness of the unreinforced collagen layer, $1 - \beta$. This is exactly the gist of the Akiva et al. (1998) model, using $u = 0.1$ nm thin layers of unmineralized between $l = 50$ nm layers of platelet-reinforced collagen. By using the unphysically small value of u (about the diameter of a single atom of hydrogen!) their model yields $E_{\text{composite}} = 33.4 E_{\text{coll}}$, which is well enough if we accept the authors' data of $E_{\text{coll}} = 1.5$ Gpa, but not enough if we use the value derived from Landis et al. (1995), $E_{\text{coll}} = 50$ Mpa $= 0.050$ Gpa (cf. Table 1). The use of the models of Padawer and Beecher (1970) or Lusis et al. (1973) is especially inappropriate in this context, because the formulae given by these authors do not even contain the all-important distance u explicitly.

Although the so-calculated values for $E_{\text{composite}}$ may just be sufficient, the main shortcoming of this model is:

$$\sigma_{\max \text{ composite}} = \sigma_{\max \text{ coll}} \quad \varepsilon_{\max \text{ composite}} = 0.004\varepsilon_{\max \text{ coll}}.$$

Both $\sigma_{\max}$ and $\varepsilon_{\max}$ are far too low compared to Table 1, depicting a very weak and brittle substance. In this model, the platelets clearly act as stress

concentrators, whereas the deformation is limited to the narrow region of matrix in between, across the axis of tension.

REFERENCES

Abe, H., K. Hayashi, and M. Sato (eds). 1996. Data Book on Mechanical Properties of Living Cells, Tissues and Organs. Springer, Tokyo, Berlin. p. 251 f and 340.

Akiva, U., H. D. Wagner, and S. Weiner. 1998. Modelling the three-dimensional elastic constants of parallel-fibred and lamellar bone: *J. Mat. Sci.* 33:1497–1509.

Arsenault, A. L., and M. D. Grynpas. 1988. Crystals in calcified epiphyseal cartilage and cortical bone of the rat: *Calcif. Tissue Int.* 43:219–225.

Carter, D. R., and W. Hayes. 1977. The compressive behavior of bone as a two-phase porous structure. *J. Bone Joint Surg.* 59A:954–962.

Currey, J. D. 1969. The relationship between the stiffness and the mineral content of bone. *J. Biomech.* 2:477–480.

Currey, J. D. 1984. The Mechanical Adaptations of Bones, Princeton Univ. Press, Princeton, N.J.

Currey, J. D. 1990. Physical characteristics affecting the tensile failure properties of compact bone. *J. Biomech.* 23:837–844.

Fratzl, P., N. Fratzl-Zelman, and K. Klaushofer. 1993. Collagen packing and mineralization. *Biophys. J.* 64:260–266.

Fratzl, P., N. Fratzl-Zelman, K. Klaushofer, G. Vogl, and K. Koller. 1991. Nucleation and growth of mineral crystals in bone studied by Small-angle x-ray scattering. *Calcif. Tissue Int.* 48:407–413.

Fratzl, P., M. Groschner, G. Vogl, H. Plenk, Jr., J. Escherberger, N. Fratzl-Zelman, K. Koller, and K. Klaushofer. 1992. Mineral crystals in calcified tissues: a comparative study by SAXS: *J. Bone Miner. Res.* 7:329–334.

Fratzl, P., K. Misof, I. Zizak, G. Rapp, H. Amenitsch, and S. Bernstorff. 1997. Fibrillar structure and mechanical properties of collagen. *J. Struct. Biol.* 122:119–122.

Fratzl, P., S. Schreiber, and K. Klaushofer. 1996. Bone mineralization as studied by small-angle x-ray scattering. *Connect. Tissue Res.* 34: 247–254.

Glimcher, M. J. 1987. The nature of the mineral component of bone and the mechanism of calcification. *Instr. Course Lect.* 36:49–69.

Hodge, A. J., and J. A. Petruska. 1963. Recent studies with the electron microscope on ordered aggregates of the tropocollagen molecule. *In* Aspects of Protein Structure, G. N. Ramachandran, editor. Academic, New York. 289–300.

Hulmes, D. J. S., T. J. Wess, D. J. Prockop, and P. Fratzl. 1995. Radial packing, order and disorder in collagen fibrils: *Biophys. J.* 68: 1661–1670.

Huiskes, R., and S. J. Hollister. 1993. From structure to precess, from organ to cell: recent developments of FE-analysis in orthopaedic biomechanics. *Trans. ASME.* 115:520–527.

Kabel, J., B. van Rietbergen, A. Odgaard, and R. Huiskes. 1999. Constitutive relationships of fabric, density, and elastic properties in cancellous bone architecture. *Bone.* 25:481–486.

Landis, W. J. 1995. The strength of a calcified tissue depends in part on the molecular structure and organization of its constituent mineral crystals in their organic matrix. *Bone.* 16:533–544.

Landis, W. J., K. J. Hodgens, J. Arena, M.-J. Song, and B. F. McEwen. 1996. Structural relations between collagen and mineral in bone by high voltage electron microscopic tomography. *Microsc. Res. Tech.* 33: 192–202.

Landis, W. J., J. J. Librizzi, M. G. Dunn, and F. H. Silver. 1995. A study of the relationship between mineral content and mechanical properties of turkey gastrocnemius tendon. *J. Bone Mineral Res.* 10:859–867.

Landis, W. J., M. J. Song, A. Leith, L. McEwen, and B. F. McEwen. 1993. Mineral and organic matrix interaction in normally calcifying tendon visualized in three dimensions by high-voltage electron microscopic tomography and graphic image reconstruction. *J. Struct. Biol.* 110: 39–54.

Lees, S. 1987. Considerations regarding the structure of the mammalian mineralized osteoid from viewpoint of the generalized packing model. *Connect. Tissue Res.* 16:281–303.

Lusis, J., R. T. Woodhams, and M. Xanthos. 1973. The effect of flake aspect ratio on the flexural properties of mica reinforced plastics. *Polymer Eng. Sci.* 13:139–145.

Misof, K., G. Rapp, and P. Fratzl. 1997. A new molecular model for collagen elasticity based on synchrotron radiation evidence. *Biophys. J.* 72:1376–1381.

Padawer, G. E., and N. Beecher. 1970. On the strength and stiffness of planar reinforced plastic resins. *Polymer Eng. Sci.* 10:185–192.

Pettermann, H. E., T. J. Reiter, and F. G. Rammerstorfer. 1997. Computational simulation of internal bone remodeling. *Arch. Comput. Meth. Eng.* 4:295–323.

Parry, D. A. D., and A. S. Craig. 1980. Growth and development of collagen fibrils in connective tissues: *In* Ultrastructure of the Connective Tissue Matrix. A. Ruggeri, P. M. Motta, editors. M. Nijhoff, Boston. 34–64.

Posner, A. S. 1987. Bone mineral and the mineralization process. *In* Bone and Mineral Research/5, W. A. Peck, editor. Elsevier Science Publ. B.V., New York, Amsterdam, Tokyo. 65–116.

Rho, J.-Y., L. Kuhn-Spearing, and P. Zioupos. 1998. Mechanical properties and the hierarchical structure of bone. *Med. Eng. Phys.* 20:92–102.

Rinnerthaler, S., P. Roschger, H. F. Jakob, A. Nader, K. Klaushofer, and P. Fratzl. 1999. Scanning small angle x-ray scattering analysis of human bone sections. *Calcif. Tissue Int.* 64:422–429.

Sasaki, N., T. Ikawa, and A. Fukuda. 1991. Orientation of mineral in bovine bone and the anisotropic mechanical properties of plexiform bone. *J. Biomech.* 24:57–61.

Veis, A., and B. Sabsay. 1987. The collagen of mineralized matrices. *In* Bone and Mineral Research/5, W. A. Peck, editor. Elsevier Science Publ. B.V., New York, Amsterdam, Tokyo. p. 15 f.

Vincent, J. F. V. 1990. Structural biomaterials. Princeton University Press. Princeton, N.J. 60.

Wagner, H. D., and S. Weiner. 1992. On the relationship between the microstructure of bone and its mechanical stiffness. *J. Biomech.* 25: 1311–1320.

Weiner, S., and H. D. Wagner. 1998. The material bone. Structure–mechanical function relations. *Annu. Rev. Material Sci.* 28: 271–298.

White, S. W., D. J. Hulmes, A. Miller, and P. A. Timmins. 1977. Collagen–mineral axial relationship in calcified turkey leg tendon by x-ray and neutron diffraction. *Nature.* 266:421–425.